DOI: 10.1002/marc.((insert number)) ((or ppap., mabi., macp., mame., mren., mats.))

Article Type: Communication

Self-assembly and surface patterning of polyferrocenylsilane-functionalized gold nanoparticles

Rachelle M. Choueiri, Anna Klinkova, Samuel Pearce, Ian Manners and Eugenia Kumacheva*

Chemical and topographic surface patterning of inorganic polymer-functionalized nanoparticles (NPs) and their self-assembly in nanostructures with controllable architectures enable the design of new NP-based materials. Capping of NPs with inorganic polymer ligands, such as metallopolymers, can lead to new synergetic properties of individual NPs or their assemblies and enhance NPs processing in functional materials. Here, for gold NPs functionalized with polyferrocenylsilane, we used two distinct triggers to induce attraction between the polymer ligands and achieve NP self-assembly or topographic surface patterning of individual polymer-capped NPs. Control of polymer-solvent interactions was achieved by either changing the solvent composition, or by the electrooxidation of polyferrocenylsilane ligands. These results expand the range of polymer ligands used for NP assembly and patterning and can be used to explore new self-assembly modalities. The utilization of electrochemical polymer oxidation stimuli at easily accessible potentials broadens the range of stimuli leading to NP self-assembly and patterning.

_____

Dr. Rachelle M. Choueiri, Department of Chemistry, University of Toronto, 80 Saint George

street, Toronto, Ontario M5S 3H6, Canada

Dr. Anna Klinkova, Department of Chemistry, University of Toronto, 80 Saint George street, Toronto, Ontario M5S 3H6, Canada

Samuel Pearce, School of Chemistry, University of Bristol, Bristol BS8 1TS, UK.

Prof., Dr. Ian Manners, School of Chemistry, University of Bristol, Bristol BS8 1TS, UK.

Prof. Dr. Eugenia Kumacheva,* Department of Chemistry, University of Toronto, 80 Saint George street, Toronto, Ontario M5S 3H6, Canada

_____

1. Introduction

Polymer-functionalized nanoparticles (NPs) have a broad range of applications, including colloidal stabilization,[1] chemical and biological sensing,[2] imaging,[3] and medical diagnostics and therapeutics.[4] In comparison with individual NPs coated with a uniform layer of polymer ligands, the self-assembly (SA) and/or the surface patterning (SP) of polymer-capped NPs provide additional versatility and level of control in the design of NP-based functional materials. Patterning of NPs with chemically and/or topographically distinct surface regions renders directionality in their interactions and self-assembly and can be used to explore new SA modes, generate colloidal surfactants[5] and produce templates for the synthesis of multicomponent, hybrid NPs. [6] Self-assembly enables the organization of NPs into nanostructures with increasingly complex architectures, which exhibit new collective optical, magnetic or electronic properties[7] due to the coupling of properties of individual NPs.

Both SA and SP can be realized for NPs capped with end-tethered polymer chains by tuning the relationship between the polymer conformational entropy and the enthalpy of its interactions with a solvent.[8] When a polymer-functionalized NP is transferred from a good to a poor solvent, polymer ligands collapse and associate with each other to reduce the free energy of the system. Figure 1 illustrates the impact of this effect for the SA and SP approaches. In both cases, the initial state of the system are NPs coated with a uniformly-thick layer of strongly solvated end-tethered polymer ligands in a good solvent. At a sufficiently high NP concentration, a reduction in solvent quality leads to the association of polymer ligands on *proximal* NPs and the formation of interparticle physical bonds, thereby producing self-assembled nanostructures.[6,9,10] Tuning the molecular weight and the grafting density of the polymer ligands, as well as the quality of the solvent enables control over interparticle spacing in the nanostructures, the characteristics that is important in chemical and biological sensing.[11,12]

The very same effect – the association of polymer ligands in a poor solvent – can be used for the SP of individual NPs. When the probability of NP collisions is reduced in dilute NP solutions, polymer association between molecules attached to the *same* NP dominates.[13] For polymers that are strongly end-grafted to the surface, surface segregation (also called constrained dewetting) leads to the formation of pinned micelles. This effect is particularly beneficial for the SP of small (~10-20 nm) NPs, which is particularly challenging to achieve. The number of pinned micelles (forming "surface patches") and their dimensions are thermodynamically controlled and can be changed by varying polymer molecular weight and grafting density, the NP size and the quality of the solvent.

Exploring the range of polymer ligands that can be used for SA and SP with a particular focus on their functionality can lead to a new and broadened range of applications of polymer-functionalized NPs in nanoscience and nanotechnology. In particular, combining optical and electrochemical properties of inorganic polymer ligands[14] with optical, electronic or magnetic properties of inorganic NPs can lead to new synergetic properties of individual NPs or their assemblies.

In addition, expanding the range of external stimuli for SA or SP can enhance the functionality of such systems. Currently, the reduction in solvent quality for polymer ligands is achieved by either adding a non-solvent to the NP solution in a good solvent, or by changing solution pH. [11] An alternative, potentially useful approach would be a stimulus-responsive change in the hydrophilic/hydrophobic properties of the polymer.

In the present work, we explored the SA and SP approaches for NPs capped with a metallopolymer ligand which combines the properties of metals with the desirable ease of polymer processing.[15] We used poly(ferrocenyldimethylsilane) (PFDMS), a member of the polyferrocenylsilane family, a class of metallocene polymers known for their interesting redox, optical, preceramic and other properties.[15-18] These polymers have been used in sensing,[19] as an electroactive component in photonic crystals,[20] as ligands for the

preparation of colloidal preceramic materials[21], and as an oxygen-plasma resistant block in block-copolymer based lithography.[22,23] Thus, we aimed to exploit the electroactive properties of new PFDMS ligands for the SA and SP of NPs.

2. Results and Discussion

The SP and SA strategies were explored for gold NPs capped with thiol-terminated PFDMS (see Figure 1). The latter was prepared in two steps which involved i) termination of living anionic PFDMS with a chloro(vinyl)silane followed by ii) attachment of the thiol group via a photochemically mediated thiol-ene "Click" reaction. Full details of the synthesis and characterization of the polymer are provided in Supporting Information. In the present work, two approaches were used to trigger attraction between the PFDMS ligands. In the first method, to reduce the quality of the solvent for the polymer, a non-solvent was added to the solution of PFDMS-capped NPs in a good solvent. In the second method, the solvophilicity of the PFDMS ligands was changed by applying an electrochemical potential to the NP solution in a good solvent and in this manner, changing the oxidation state of the ferrocene groups.[24] The parameter space for the SA and SP for PFDMS-functionalized gold NPs included the change in temperature, the time, the solvent composition and the magnitude of the electrochemical potential. The PFDMS-functionalized NPs exhibited both SA and SP behavior, which yielded single-patch Janus NPs and self-assembled NP clusters.

Gold NPs with dimensions of either 20, or 40 nm were synthesized using a procedure reported elsewhere.[25] Following NP synthesis, the surfactant cetyltrimethylammonium bromide was replaced with thiol-terminated PFDMS with a weight average molecular weight, M_w, of 36 100 g/mol (Figures S1-3, Supporting information) *via* a ligand exchange procedure. An aqueous solution of as-synthesized gold NPs was concentrated from 1.5 mL solution to ~ 30 µL using 15 min centrifugation at 5000 *g* at 27°C and subsequent removal of the supernatant. The concentrated NP solution was sonicated for 5 s and added to 1.5 mL of the

dilute solution of thiol-terminated PFDMS in tetrahydrofuran (THF). The resulting solution was maintained undisturbed at room temperature overnight. Then, the NPs were separated from free (non-attached) PFDMS *via* one cycle of centrifugation of the solution (15 min, 5000 *g*, 20 °C), removal of the supernatant, and dilution of the solution with THF. Successful exchange of cetyltrimethylammonium bromide with PFDMS was verified by the colloidal stability of the NPs in THF, a poor solvent for cetyltrimethylammonium bromide. In addition, an increase in the apparent hydrodynamic radius of the NPs after functionalization with PFDMS was observed due to the engulfment of the NPs with a polymer corona (Figure S4, Supporting Information). The extinction spectra of the PFDMS-capped NPs did not exhibit a significant shift in the surface plasmon resonance after ligand exchange (Figure S5, Supporting information).

The PFDMS-capped NPs were transferred from THF to chloroform, a good solvent for PFDMS (a Hildebrand solubility parameter, δ, of ~19.0 $MPa^{1/2}$ of chloroform is close to that of PFDMS of 18.7 $MPa^{1/2}$).[26] To reduce the solvent quality, cyclohexane with $\delta = 16.8$ $MPa^{1/2}$ (a non-solvent for PFDMS),[27-29] was added dropwise to the solution of PFDMS-capped NPs in chloroform. The volume fraction, φ, of cyclohexane in the solution was varied from 0 to 0.75.

Subsequently to incubation of PFDMS-capped NPs in a poor solvent, a droplet of the NP solution was deposited on a carbon-coated copper mesh grid. The NPs were imaged using a Hitachi H-7000 transmission electron microscope. Figure 2a shows transmission electron microscopy (TEM) images of the arrays of PFDMS-capped 20 nm-diameter NPs deposited on a carbon-coated grid from chloroform/cyclohexane solutions with varying φ. In chloroform (φ=0), a uniform 13 ± 3 nm distance between the NPs served as the indication of a PFDMS "shell" acting as a spacer between the gold core. The grafting density, σ, of PFDMS on these NPs was estimated as [30]

$$\sigma = \frac{h\rho N_A}{M_n} \quad , \qquad (1)$$

where h is the average height of the brush measured from TEM images (taken as half of the inter-particle distance, h≈6.5 nm), ρ is the density of PFDMS (ρ≈1.3 g/mL),[31] and N_A is Avogadro's number. For 20 nm-diameter NPs, the estimated σ was 0.14 polymer chains/nm^2. With increasing φ, the inter-particle distance decreased, consistent with a reducing solvent quality. This effect is quantitatively presented in Figure 2b, where the interparticle distance reduced from ~13 to ~5 nm with φ increasing from 0 to 0.75, respectively. The reduction in interparticle distance served as an indication of the collapse of the PFDMS ligands in a poor solvent, with a degree of collapse increasing with reducing solvent quality. At high values of σ, brush collapse in a poor solvent resulted in a uniformly thick polymer shell around NPs and regular interparticle distances.

The results shown in Figure 2c, in conjunction with the results of dynamic light scattering experiments (showing the formation of NP clusters in a poor solvent) (Fig. S6, Supporting Information) pointed to the capability of PFDMS-functionalized NPs to undergo self-assembly, as shown in Figure 1, top and consistent with our previous results for the SA of polystyrene-capped gold NPs in a poor solvent.[8]

The SP and SA approaches of PFDMS-capped NPs in the chloroform/cyclohexane solutions was explored at 20, 40, and 60°C. Moderate temperatures ≤80 °C were required to avoid irreversible NP agglomeration and evaporation of the solvent. For temperatures <60 °C, PFDMS segregation on the NP surface was not observed, even after 12 h-long incubation time (Figure S7, Supporting Information). The optimized conditions - heating the NP solution in a chloroform/cyclohexane mixture at φ≥0.5 at 60°C for 15 min - were used, similar to the methodology developed in SA experiments for PFDMS-containing block copolymers.[31]

The interplay between poor solvent-induced SA and SP was further explored for 40 nm-size of PFDMS-stabilized NPs in solutions with ten-fold difference in NP concentration, C_{NP}.

Nanoparticle concentrations in the solution were determined in ultraviolet-visible spectroscopy experiments, whereby the solution extinction was related to NP concentration by using previously determined molar extinction coefficients for gold NPs.[10] Using Eq. 1, the PFDMS grafting density, σ, for 40 nm-diameter NPs was estimated to be 0.11 chains/nm^2, that is, lower than for PFDMS-capped 20 nm NPs.

Figure 3a shows representative TEM images of the self-assembled nanostructures formed by PFDMS-functionalized NPs in the chloroform/cyclohexane mixture at φ=0.5 at C_{NP}=10 nM. In solutions, based on the results of dynamic light scattering, the NPs formed clusters with the average size of 337 ± 40 nm (Figure S6, Supporting Information). This self-assembly mode was similar to the SA of polystyrene-capped gold NPs in solvents with a low dielectric constant.[8]

In dilute solutions of PFDMS-functionalized NP at C_{NP}=1 nM and φ=0.5 we observed PFDMS segregation into a patch on the surface of individual NPs, as shown in a representative TEM image in Figure 3b. Qualitatively, the morphology of NPs with a patterned surface was similar to that observed for polystyrene-capped NPs in a poor solvent at polymer grafting density below a threshold value.[11] We note that the intrinsic condition of SP experiments was a low value of CNP and thus low-magnification TEM images for NPs with a patterned surface were not helpful due to the low NP density. The average hydrodynamic diameter of patchy NPs was 79 ± 5 nm, comparable to the hydrodynamic diameter of as-prepared PFDMS-tethered NPs. Importantly, due to the lower polymer grafting density on the surface of 40 nm NPs than on 20 nm NPs, PFDMS ligands formed patches, rather than undergoing uniform collapse in a poor solvent, as shown in Figure 2a, in agreement with our earlier work.[13]

In the next step, to explore the SA and SP strategies for PFDMS-functionalized NPs we utilized an electrochemical stimulus. We rationalized that when an appropriate

overpotential is applied to solutions of PFDMS-capped NPs, the iron centers on the backbone of PFDMS ligands would be oxidized, thereby changing the solvophobicity of PFDMS.

A three-electrode cell comprising a platinum counter electrode, a silver wire reference electrode and a disposable carbon paper working electrode was custom-made. The PFDMS-capped NPs were dispersed at a concentration of ~1 nM in dichloromethane with 0.1 M tetraethylammonium tetrafluoroborate (TEATFB) used as a supporting electrolyte. This solution is commonly utilized as a supporting electrolyte solution in electrochemistry experiments of PFDMS.[34] Cyclic voltammetry and chronoamperometry experiments were performed using an Autolab potentiostat with magnetic stirring. As a control system, we used a solution of free PFDMS polymer in 0.1 M solution of TEATFB in DCM.

In Figure 4a, a blue-color cyclic voltammogram (CV) curve displays the reversible two-step oxidation of PFDMS.[22] Analogously to ferrocene, under an applied potential the iron (II) centers in PFDMS underwent one electron oxidation to form iron (III) at the anode. The first and the second oxidation peaks corresponded to the oxidation of alternating and adjacent ferrocene centres, respectively, indicating repulsive interaction between the electroactive centers in the polymer[20,33] The oxidation of iron centers occurred step-wise, because a ferrocenium group increases the oxidation potential of the neighboring unoxidized ferrocene centers and thus make its oxidation energetically unfavourable. Similarly, the reduction of the positive iron centers occurred in two steps and was reversible.

Similarly to free PFDMS, the CV curve of PFDMS-functionalized NPs in 0.1 M TEATFB solution in DCM exhibited the characteristic reversible two-peak oxidation of PFDMS (red trace). The positions of oxidation peak maxima for PFDMS-NPs were similar to those for free PFDMS polymer, however, the reduction peaks were shifted to higher potentials. Further investigation is required to explore the origin of this shift.

In the next step, we conducted chronoamperometric (CA) experiments for both free PFDMS polymer and for the PFDMS-coated NPs in 0.1 M TEATFB solution in DCM (Figure

4b, blue and red traces, respectively). Experiments were carried out at the oxidation potential of +0.7 V, that is, at the maximum for the second oxidation peak. For both systems, the initial current was on the order of tens of microamperes. In the course of the experiment, the current gradually decreased due to the PFDMS oxidation, thereby leading to the loss of colloidal stability of the NPs and their subsequent deposition on the working electrode. This process was marked by a change of the solution colour from light pink to colourless.

After 10 min, the CA process was stopped, a small section of the carbon paper electrode was cut, mounted on a stub and imaged using SEM. Both individual NPs with a PFDMS patch (Figure 4d) and three-dimensional NP clusters (Figure 4c) were observed, being adhered to the carbon fibers of the electrode. At the beginning of the CA experiment, individual patchy PFDMS-coated NPs were present in larger amount, however as the PFDMS oxidation proceeded, a larger number of clusters was observed, as individual PFDMS-capped NPs became colloidally unstable in the electrode vicinity. After 30 min, large-scale NP aggregation dominated.

Figure 4c shows NP clusters formed by the association of PFDMS-capped NPs due to the loss in solubility of electrooxidized PFDMS next to the electrode and subsequent cluster precipitation of the electrode surface. The appearance of these clusters was similar to that of the assemblies of PFDMS-tethered NPs formed in the cyclohexane/chloroform mixture. The average size of NP clusters formed by electrooxidation-induced SA was 50 ± 13 nm. Figure 4d shows single-patch PFDMS-capped NPs. Patches were formed due to the formation of pinned micelles by electrooxidized PFDMS.

3. Conclusions

In summary, solution-based SA of PFDMS-capped gold NPs in clusters and topographic SP of individual PFDMS-capped gold NPs were achieved by triggering attraction between PFDMS ligands in a poor solvent. Two methods were used to change the solvent quality for

PFDMS: addition of a non-solvent to the NP solution in a good solvent and electrooxidation of PFDMS. These results broaden the range of polymer ligands used for NP assembly and enable new SA modalities of "colloidal molecules". On the other hand, the use of electrochemical redox triggers operating at easily accessible potentials expands the range of stimuli that can be used for SA and SP of NPs. By expanding the range of stimuli available for SP and SA of NPs, it may be possible to trigger the SP or SA of specific NP building blocks in a mixture of NPs on-demand, which may further facilitate the generation of nanostructures with complex architectures and new optical or other properties.

Supporting Information. Synthesis of gold NPs, synthesis of thiol-terminated PFDMS, experimental details on functionalization of gold NPs with thiol-terminated PFDMS and reparation of patchy PFDMS-functionalized gold NPs. The following files are available free of charge.

Author Information. Corresponding Author Eugenia Kumacheva, ekumache@chem.utoronto.ca

Acknowledgements

The authors thank NSERC Canada (Discovery Grant) for financial support of this work. EK thanks Canada Research Chair program (NSERC Canada).

Received: Month XX, XXXX; Revised: Month XX, XXXX; Published online:

Keywords: nanoparticles, metallopolymer, polyferrocenylsilane, nanopaterning, self-assembly

References

[1] B. P. Binks, *Curr. Opin. Colloid Interface Sci.* **2002**, *7*, 21.

[2] N. Uehara, *Anal. Sci*. **2010**, *26*, 1219.

[3] S. K Nune,; P. Gunda, P. K. Thallapally, Y. Lin, M. Laird,; C. J. Berkland, *Expert Opin. Drug Deliv.*, **2009**, *6*, 1175.

[4] S. K. Yen, P. Padmanabhan, S. T. Selvan. *Theranostics* **2013**, *3*, 986.

[5] L. C. Bradley, W.-H. Chen, K. L. Stebe, D. Lee, D. *Curr. Opin. Coll. Interface Sci.*, **2017**, *30*, 25.

[6] T. Chen, G. Chen, S. Xing, T. Wu, H. Chen, H. *Chem. Mater*. **2010**, *22*, 3826.

[7] Z. Nie, A. Petukhova and E. Kumacheva. *Nat. Nanotechnol*. **2010**, *5*, 15–25

[8] R. M. Choueiri, A. Klinkova, H. Thérien-Aubin, M. Rubinstein, E. Kumacheva, *J. Am. Chem. Soc*., **2013**, *135*, 10262.

[9] R. M. Choueiri, E. Galati, A. Klinkova, H. Thérien-Aubin, E. Kumacheva. *Faraday Discuss*. **2016**, *191*, 189.

[10] A. Sánchez-Iglesias, M. Grzelczak, T. Altantzis, B. Goris, J. Pérez-Juste, S. Bals, G. Van Tendeloo, S. H. Donaldson, B. F. Chmelka, J. N. Israelachvili and L. M. Liz-Marzán, *ACS Nano* **2012**, *6*, 11059.

[11] . A. Lee, G. F. S. Andrade, A. Ahmed, M. L. Souza, N. Coombs, E. Tumarkin, K. Liu, R. Gordon, A. G. Brolo, E. Kumacheva, *J. Am. Chem. Soc*. **2011**, *133*, 7563.

[12]. A. Klinkova, H. Thérien-Aubin, A. Ahmed, D. Nykypanchuk, R. M. Choueiri, B. Gagnon, A. Muntyanu, O. Gang, G. C. Walker , E. Kumacheva, *Nano Lett*. **2014**, *14*, 6314.

[13]. R. M. Choueiri, E. Galati, H. Thérien-Aubin, A. Klinkova, E. M. Larin, A. Querejeta-Fernández, L. Han, H. L. Xin, O. Gang, E. B. Zhulina, M. Rubinstein , E. Kumacheva. *Nature* **2016**, *538*, 2.

[14] G. R. Whittell, M. D. Hager, U. S. Schubert, I. Manners. *Nat. Mater*. **2011**, *10*, 176.

[15]. a) R. L. N. Hailes, A. M. Oliver, J. Gwyther, G. R. Whittell, I.. Manners. *Chem. Soc.*

Rev., **2016**, *45*, 5358; b) V. K. Bernhard, J. Schmidt, J. Elbert, D. Scheid, C. J. Hawker, D. Klinger, M. Gallei. *ACS Macro Lett*. **2015**, *4*, 731; c) M. Peter, R. G. H. Lammertink, M. A. Hempenius, M. van Os, M. W. J. Beulen, D. N. Reinhoudt, W. Knoll, G. J. Vancso, *Chem. Commun*., **1999**, 359.

[16]. M. J. MacLachlan, M. Ginzburg, N. Coombs, G. A. Ozin, I. Manners. *J. Am. Chem. Soc*. **2000**, *122*, 3878.

[17] a) R. Pietschnig, *Chem. Soc. Rev*. **2016**, *45*, 5216; b) L. Thomi, P. Schaefer, K. Landfester, F. R. Wurm. *Macromolecules* **2016**, *49* , 105.

[18] C. Paquet, P. W. Cyr, E. Kumacheva, I. Manners, *Chem. Comm*. **2004**, 234.

[19]. X. Sui, X. Feng, J. Song, M. A. Hempenius, G. J. Vancso, *J. Mater. Chem*. **2012**, *22*, 11261.

[20] D. P. Puzzo, A. C. Arsenault, I. Manners, G. A. Ozin, *Angew. Chem. Int. Ed*. **2009**, 48, 943.

[21] J. Elbert, H. Didzoleit , C. Fasel, E. Ionescu, R. Riedel, B. Stühn, M. Gallei. Macromol. Rapid Commun. **2015**, *36*, 597.

[22] R. G. H. Lammertink, M. A. Hempenius, V. Z.-H. Chan, E. L. Thomas and G. J. Vancso, Chem. Mater., **2001**, *13*, 429.

[23] . V. P. Chuang, J. Gwyther, R. A. Mickiewicz, I. Manners, C. A. Ross, *Nano Lett*. **2009**, *9*, 4364.

[24] M. Péter, R. G. H. Lammertink, M. A. Hempenius. G. J. Vancso, *Langmuir* **2005**, *21*, 5115.

[25] N. R. Jana, L. Gearheart and C. J. Murphy, *Langmuir* **2001**, *17*, 6782.

[26] K. Kulbaba, M. J. MacLachlan, C. E. B. Evans, I. Manners, *Macromol. Chem. Phys.* **2001**, *202*, 1768.

[27]. Allan F.M. Barton, *CRC Handbook of Solubility Parameters and Other Cohesion Parameters*, 2-nd Edition, CRC Press, 1991, 768 pages.

[28] D. M. Koenhen, C. A. Smolders, *J. Appl. Polym. Sci*. **1975**, *19*, 1163.

[29] J. Qian, Y. Lu, A. Chia, M. Zhang, P. A. Rupar, N. Gunari, G. C. Walker, G. Cambridge, F. He, G. Guerin, I. Manners, M. A. Winnik, *ACS Nano* **2013**, *7*, 3754.

[30] W. J. Brittain and S. Minko, *J. Polym. Sci. Part A Polym. Chem*. **2007**, *45*, 3505.

[31] A. Nunns, G. R. Whittell, M. A. Winnik, I. Manners, *Macromolecules* **2014**, *47*, 8420.

[32] C. Paquet; P. W. Cyr, E. Kumacheva, I. Manners, I. *Chem. Mater*. **2004**, *16*, 5205

[33]. X.-J. Wang, L. Wang, J. Wang, T. Chen, *J. Appl. Polym. Sci*. **2007**, *103*, 789.

[34]. R. Rulkens, A. J. Lough, I. Manners, S.R. Lovelace, C. Grant, W. E. Geiger, *J. Am. Chem. Soc*. **1996**, *118*, 12683.

.

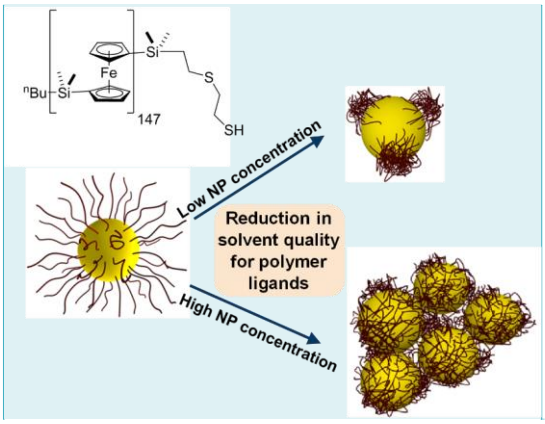

Commented [IM1]: Figure 1 changed by Ian

Figure 1. Structure of thiol-terminated PFDMS (top left), schematic of self-assembly, SA (middle-top) and surface patterning, SP (middle-bottom) of polymer-capped NPs, both triggered by a decrease in solvent quality for the polymer ligands.

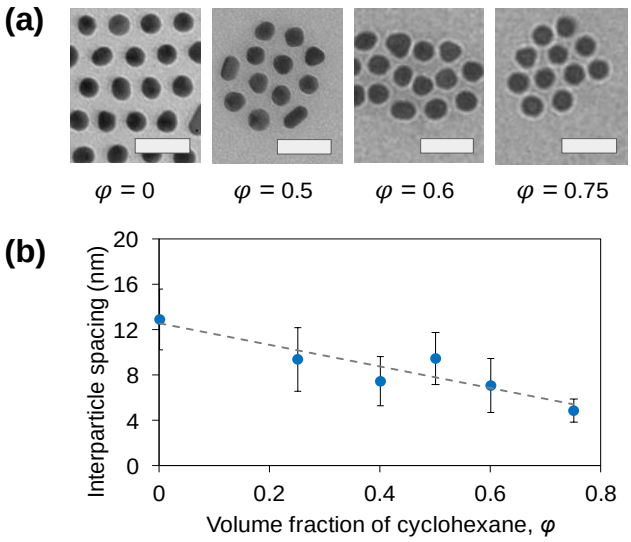

Figure 2. Effect of solvent quality on interparticle distance. (a) TEM images of PFDMS-tethered NPs deposited of the grid from chloroform/cyclohexane solution with varying volume fraction of cyclohexane, ϕ. Scale bars are 50 nm. (b) Variation in the average interparticle distance with ϕ. The 10 nM solution of PFDMS-capped NPs was subjected to heating at 60°C for 15 min.

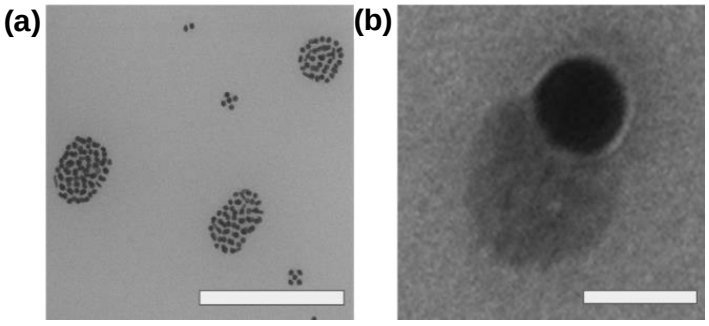

Figure 3. TEM images of PFDMS-capped gold NPs (a) Self-assembled nanostructures formed by PFDMS-functionalized gold NPs at C_{NP}=10 nM. Scale bar 500 nm. (b) TEM image of an individual gold PFDMS-capped NP patterned with a PFDMS patch. Scale bar 50 nm. C_{NP}=1 nM. Both SA and SP were performed in the chloroform/cyclohexane mixture (φ=0.5) upon heating at 60 °C for 15 min.

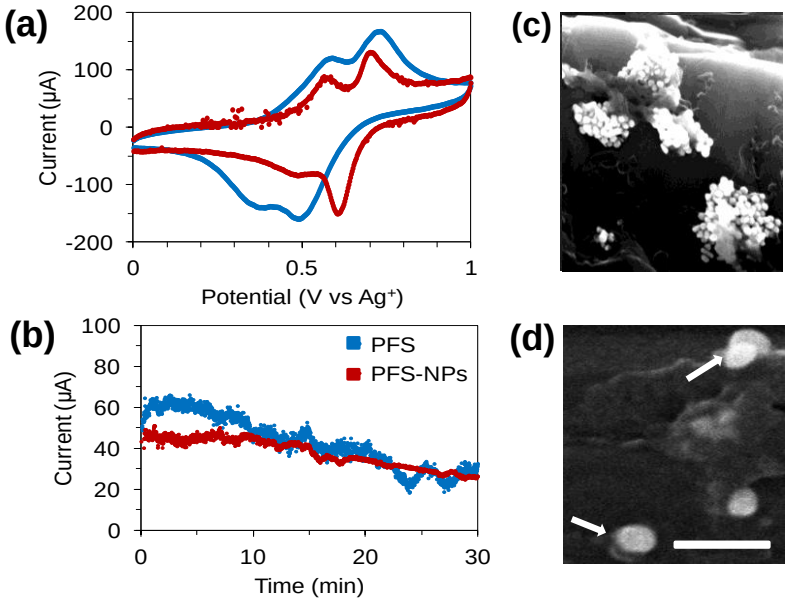

Figure 4. Electrooxidation-induced SA and SP of PFDMS-capped gold NPs (a) Cyclic voltammograms of PFDMS polymer (blue) and PFDMS-functionalized gold NPs (red) in 0.1M TEATFB electrolyte solution in DCM. Sweep rate 200 mV/s. (b) PFDMS oxidation at +0.7 V over 30 min for PFDMS (blue) and PFDMS-capped gold NPs (red) in 0.1M TEATFB electrolyte solution in DCM. (c, d) Representative SEM images of (c) PFDMS-stabilized Au NPs on the carbon paper electrode coated with clusters of PFDMS-NPs after 30 min oxidation at +0.7 V applied potential relative to Ag/Ag+ and (d) individual PFDMS-stabilized Au NPs on the carbon paper electrode after 10 min oxidation at +0.7 V applied potential relative to Ag/Ag+. Scale bars are 250 nm in (c) and 100 nm in (d).

Rachelle M. Choueiri, Anna Klinkova, Samuel Pearce, Ian Manners and Eugenia Kumacheva*

Self-assembly and surface patterning of polyferrocenylsilane-functionalized gold nanoparticles

The table of contents entry: Surface patterning and self-assembly of gold nanoparticles capped with metallopolymer polyferrocenylsilane have been achieved by applying two distinct external stimuli. Change in solvent composition and polymer electrooxidation induced attraction between the polymer ligands. These results expand the range of polymers and stimuli used for nanoparticle patterning and enable the exploration of new self-assembly modalities.

ToC figure

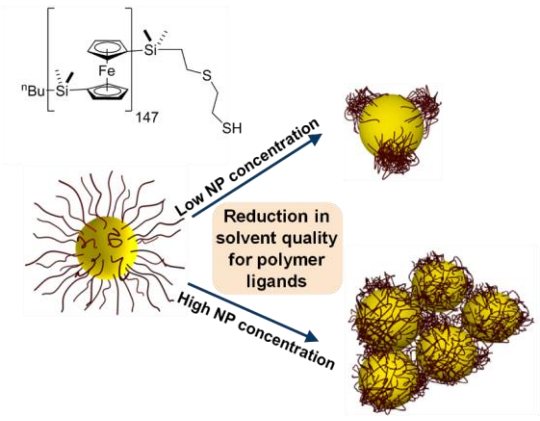

Supporting Information

DOI: 10.1002/marc.2013#####

Self-assembly and surface patterning of polyferrocenylsilane-functionalized gold nanoparticles

Rachelle M. Choueiri[a], Anna Klinkova[a], Samuel Pearce[b], Ian Manners[b], Eugenia Kumacheva[a,c,d,*]

1. Synthesis of gold nanoparticles

Spherical gold nanoparticles (NPs) with a diameter of 19 ± 1 nm were synthesized using a two-step seed-mediated procedure reported elsewhere[1]. A seed solution was prepared by reducing $HAuCl_4$ (10 mL, $5x10^{-4}$ M) in 10 mL of aqueous citrate solution (5×10^{-4} M) *via* the addition of ice-cold solution of $NaBH_4$ in water (0.6 mL, 0.1 M) under stirring. The stirring was stopped 10 min after the addition of $NaBH_4$ solution, and the resultant solution was stored at room temperature for 2-3 h. A second solution, denoted as "Solution A" was prepared by dissolving $HAuCl_4$ (2.5×10^{-3}M) and cetyltrimethylammonium bromide (CTAB) (0.08 M) in water. An aqueous solution of ascorbic acid (0.5 mL, 0.1 M) was added to 9 mL of Solution A. Immediately after that, 10 mL of the aged seed solution was added to the above mixture under vigorous stirring. The resultant solution (Solution B) was stirred for 10 min and used 30 min after its preparation. Another solution, denoted as "Solution C", was prepared by dissolving $HAuCl_4$ (2.5×10^{-3} M) and CTAB (0.08 M) in water. An aqueous solution of ascorbic acid (0.5 mL of 0.1 M) was added to 9 mL of Solution C. Following this step, 9 mL of Solution B was added under vigorous stirring for 10 min. The resultant solution containing NSs was incubated at room temperature overnight.

Spherical gold NPs with an average diameter of 40 nm were synthesized using a several-step procedure and subsequent etching. The latter step was used to produce NPs with close-to-spherical shape. Seed gold NPs were prepared using a method reported elsewhere[2,3]. A solution of freshly prepared, ice-cold $NaBH_4$ in deionized water (10 mM, 0.6 mL) was added under stirring to a solution prepared by mixing aqueous CTAB (0.1 M, 9.833 mL) and $HAuCl_4$ (15 mM, 0.167 mL) in a 20 mL scintillation vial, thereby forming a seed solution. After 2 min stirring, the pale yellow seed solution was left undisturbed at room temperature for 2 h. This solution was then diluted to 100 mL with deionized water. In another flask, growth solution was prepared by combining aqueous solutions of CTAB (0.24 M, 4 mL) with $HAuCl_4$ (15 mM, 0.133 mL) and ascorbic acid (0.1 M, 3 mL). The resulting clear solution was subsequently diluted to 50 mL with deionized water. To this solution, 0.6 mL of the diluted seed solution was added and the resulting mixture was shaken vigorously, resulting in a pale pink-coloured solution. The resultant solution was left undisturbed at room temperature for 12 h. Excess surfactant from this solution was removed by using one cycle of centrifugation (20,000 g, 20 min, 28°C), removing the supernatant and redispersing NS seeds with deionized water. Later in the text, this solution is referred to as a "purified seed solution". To prepare 40 nm-diameter NSs, 5 mL of the purified seed solution, was added to a 20 mL scintillation vial and diluted it to 10 mL with deionized water. Then, 1.6 mL of aqueous surfactant solution (0.1 M CTAB) was added to this solution. The resultant solution was heated to 30ºC in a water bath for 5 min. The solution was removed from the water bath and 250 μL of 15 mM aqueous $HAuCl_4$ solution and 0.8 mL of 0.1 M ascorbic acid were added in succession. The NPs were left undisturbed at room temperature for 15 min. This synthesis was scaled up to obtain up to 500 mL of NP solution.

2. Synthesis of thiol-terminated polyferrocenyldimethylsilane (PFDMS)

Synthesis of vinyl-capped PFDMS homopolymer

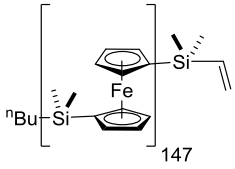

Within a nitrogen-filled glove box, dimethylsila[1]ferrocenophane (500 mg, 2.06 mmol) was dissolved in dry, degassed THF (3 mL) in a Schlenk tube capped with a Young's tap. The solution was stirred rapidly at room temperature, and the polymerisation initiated with n-butyllithium (1.6 M in hexanes, 15.8 x10^{-3} mmol, 9.85 µL). The reaction mixture was left for 30 min, during which the colour of the solution turned from dark red to amber, and was then removed from the glovebox and capped with chlorodimethylvinylsilane (0.1 mL) under N_2 on a Schlenk line. Polymer purification was conducted by 3 precipitations in methanol, from polymer solution in THF. The pure product was obtained as an orange solid in high yield (95%). ^{1}H NMR (cryo 500 MHz, δ, C_6D_6): 5.7-6.4 (m, 3H, $Si(CH_3)_2C\underline{H}C\underline{H}_2$), 4.28 (m, 588H, Cp$\underline{H}$), 4.12 (m, 588H, Cp$\underline{H}$), 0.56 (s, 882H, $SiC\underline{H}_3$) M_n (MALDI-TOF) = 36.1 kg mol^{-1} M_w/M_n (GPC) = 1.10.

Synthesis of thiol-terminated PFDMS homopolymer

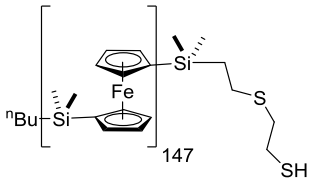

Within glovebox, under nitrogen atmosphere, vinyl-capped PFDMS homopolymer (450 mg, 12.5 µmol) was dissolved in THF (3 mL), within a Youngs tube, to form a light amber solution. To this solution, photoinitiator 2,2-dimethoxy-2-diphenylacetophenone (5 mg) was added. The Young's tube was then sealed and removed from the glove box and attached to a Schlenk line. 1,2,-ethanedithiol (0.1 mL, 1.19 x10^{-3} moles) was added via degassed syringe under inert atmosphere. The sealed Youngs tube was then UV-irradiated under inert

atmosphere, at room temperature for 2 hrs. The reaction product was purified by sequential precipitations into degassed hexane from a solution of polymer in THF, to prevent oxidative coupling of the thiol termini. The pure product was obtained as an orange powder in moderate yield (50%). End group conversion was confirmed by ^{1}H NMR as no vinyl proton chemical shifts were detected. ^{1}H NMR (cryo 500 MHz, δ, C_6D_6): 4.28 (m, 588H, CpH), 4.12 (m, 588H, CpH), 2.3-2.80 (m, 6H,$CH_2SCH_2CH_2$), 1.02 (m, 2H, $(CH_3)_2SiCH_2CH_2$), 0.56 (s, 882H, $SiCH_3$) M_n (MALDI-TOF) = 35.3 kg mol^{-1} (see Figure S3 and the caption for peak assignments which are fully consistent with the expected structure).

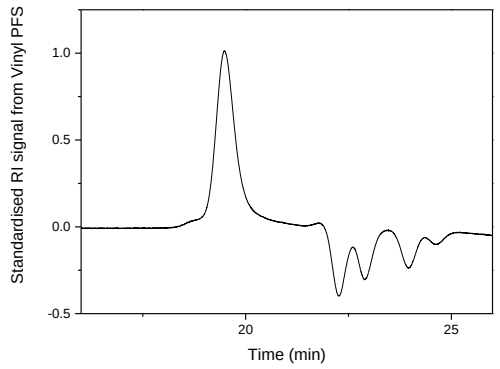

Figure S1. GPC trace of vinyl-terminated $PFDMS_{147}$

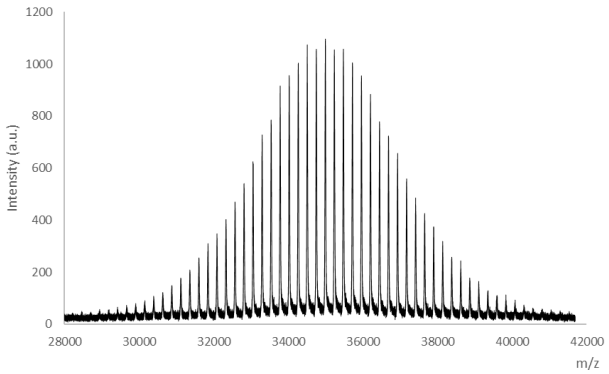

Figure S2. MALDI-TOF mass spectrum of vinyl-terminated $PFDMS_{147}$. The spacing between the peaks corresponds to 242, the repeat unit of PFDMS.

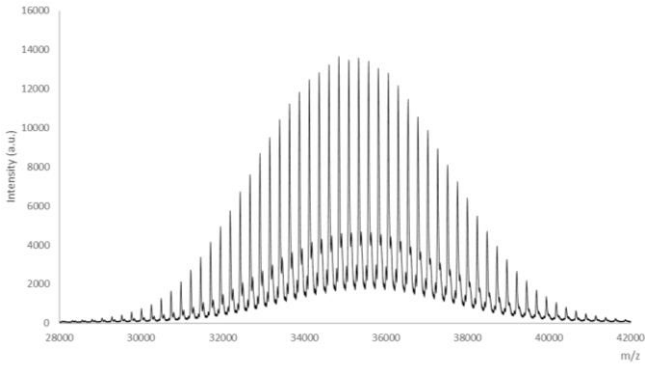

Figure S3. MALDI-TOF mass spectrum of thiol-terminated $PFDMS_{147}$. The spacing between the major peaks corresponds to 242, the repeat unit of PFDMS. The spectrum consists of 3 sets of peaks assigned as (on moving to lower molar mass): PFDMS-$SiMe_2CH_2CH_2SCH_2CH_2SH$ (low intensity), PFDMS-$SiMe_2CH_2CH_2S$ (major peak, loss of 61 amu) and PFDMS-$SiMe_2$ (very low intensity, further loss of 60 amu).

3. Functionalization of gold NPs with thiol-terminated PFDMS

Figure S4 shows the normalized intensity of dynamic light scattering for CTAB-coated and PFDMS-coated gold NPs dispersed in water and THF, respectively. The hydrodynamic diameter of the NPs increased upon functionalization with PFDMS, indicating a successful ligand exchange.

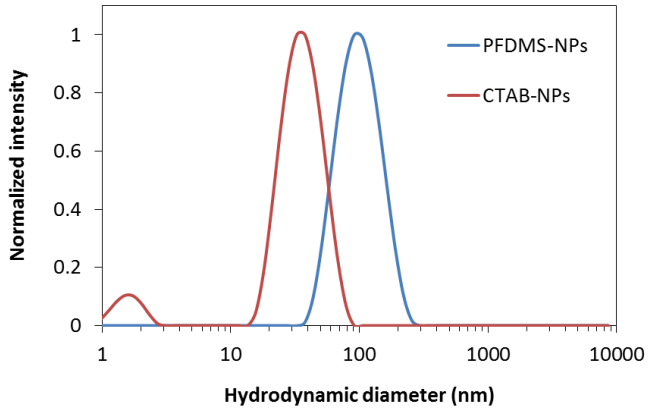

Figure S4. Hydrodynamic diameter of CTAB- and PFDMS-coated gold NPs measured in water and THF, respectively.

Figure S5 shows extinction spectra of PFDMS, CTAB-coated NPs, PFDMS-capped NPs, and PFDMS-capped NPs after washing. The peak for free PFDMS at ~450 nm evident in the extinction spectrum of PFDMS-functionalized NPs, however, the intensity decreased significantly after one purification cycle *via* centrifugation.

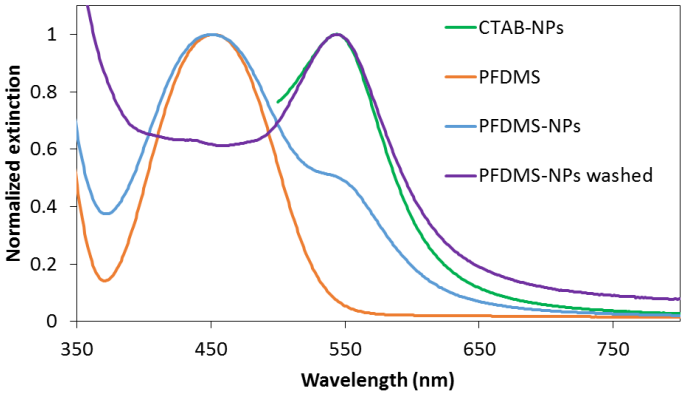

Figure S5. Normalized extinction spectra of CTAB-functionalized 40 nm NPs in water, PFDMS free polymer in THF, PFDMS-functionalized 40 nm gold NPs in THF, and PFDMS-NPs in THF after one purification cycle *via* centrifugation.

4. Preparation of patchy PFDMS-functionalized gold NPs

100 µL of the solution of purified PFDMS-functionalized gold NPs was dried in a 20 mL scintillation vial and subsequently, redispersed in 200 µL of chloroform. To this solution, 200 µL of cyclohexane was added dropwise, resulting in a solution composed of 1:1 vol/vol of chloroform and cyclohexane. The resultant NP solution was incubated at 60°C in a recirculating water bath for 60 min, unless otherwise stated.

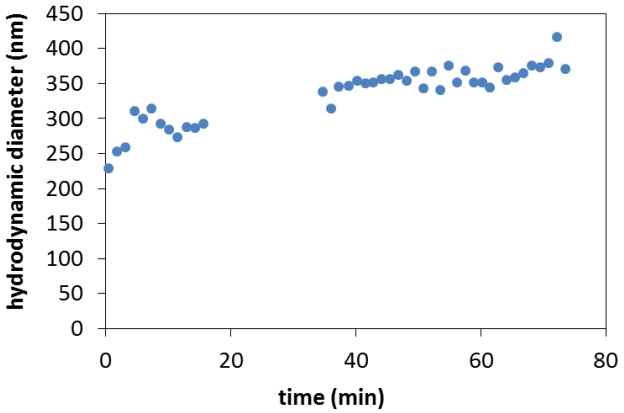

*Figure S6***.** Variation in the hydrodynamic diameter of NP clusters with self-assembly time.

5. Effect of temperature on SP and SA of PFDMS-capped NPs

The effect of temperature, *T*, on PFDMS-capped NPs suspended in the 1:1 vol/vol cyclohexane/chloroform mixture was explored for *T* of 20, 40, and 60°C for incubation times, *t* of 15 min, 30 min, 1 h and 12 h. Experiments were conducted as described in Section 4. The samples for TEM imaging were prepared immediately after the completion of the incubation period.

Figure S7 shows TEM images of PFDMS-capped NSs in 1:1 vol/vol cyclohexane/chloroform after 12 h of incubation at 20 and 40°C. Polymer surface segregation did not occur under these conditions, as can be seen from the images.

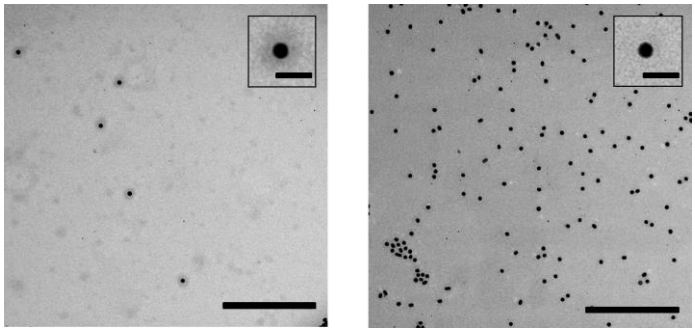

*Figure S7***.** Representative TEM images of PFDMS-capped NPs after incubation in the 1:1 vol/vol cyclohexane/chloroform mixture at T = 20°C for t = 12 h (left) and at T = 40°C for t = 12 h (right). Scale bars are 500 nm. The insets show high-magnification images of representative PFDMS-coated NPs with no segregation in the polymer shell after incubation. Insets: scale bars are 50 nm.

References

[1]. N. R. Jana, L. Gearheart and C. J. Murphy, *Langmuir* **2001**, *17*, 6782.

[2]. F.-R. Fan, D.-Y. Liu, Y.-F. Wu, S. Duan, Z.-X. Xie, Z.-Y. Jiang, Z.-Q. Tian, *J. Am. Chem. Soc*., **2008**, *130*, 6949.

[3].. F. Lu, Y. Tian, M. Liu, D. Su, H. Zhang, A. O. Govorov, O. Gang, *Nano Lett*., **2013**, *13*, 3145.